



Chemistry A European Journal

 **Chemistry
Europe**
European Chemical
Societies Publishing

Accepted Article

Title: Design approach of lifetime extending thermally activated delayed fluorescence sensitizers for highly efficient fluorescence devices

Authors: Sung Joon Yoon, Ji Han Kim, Won Jae Chung, and Jun Yeob Lee

This manuscript has been accepted after peer review and appears as an Accepted Article online prior to editing, proofing, and formal publication of the final Version of Record (VoR). This work is currently citable by using the Digital Object Identifier (DOI) given below. The VoR will be published online in Early View as soon as possible and may be different to this Accepted Article as a result of editing. Readers should obtain the VoR from the journal website shown below when it is published to ensure accuracy of information. The authors are responsible for the content of this Accepted Article.

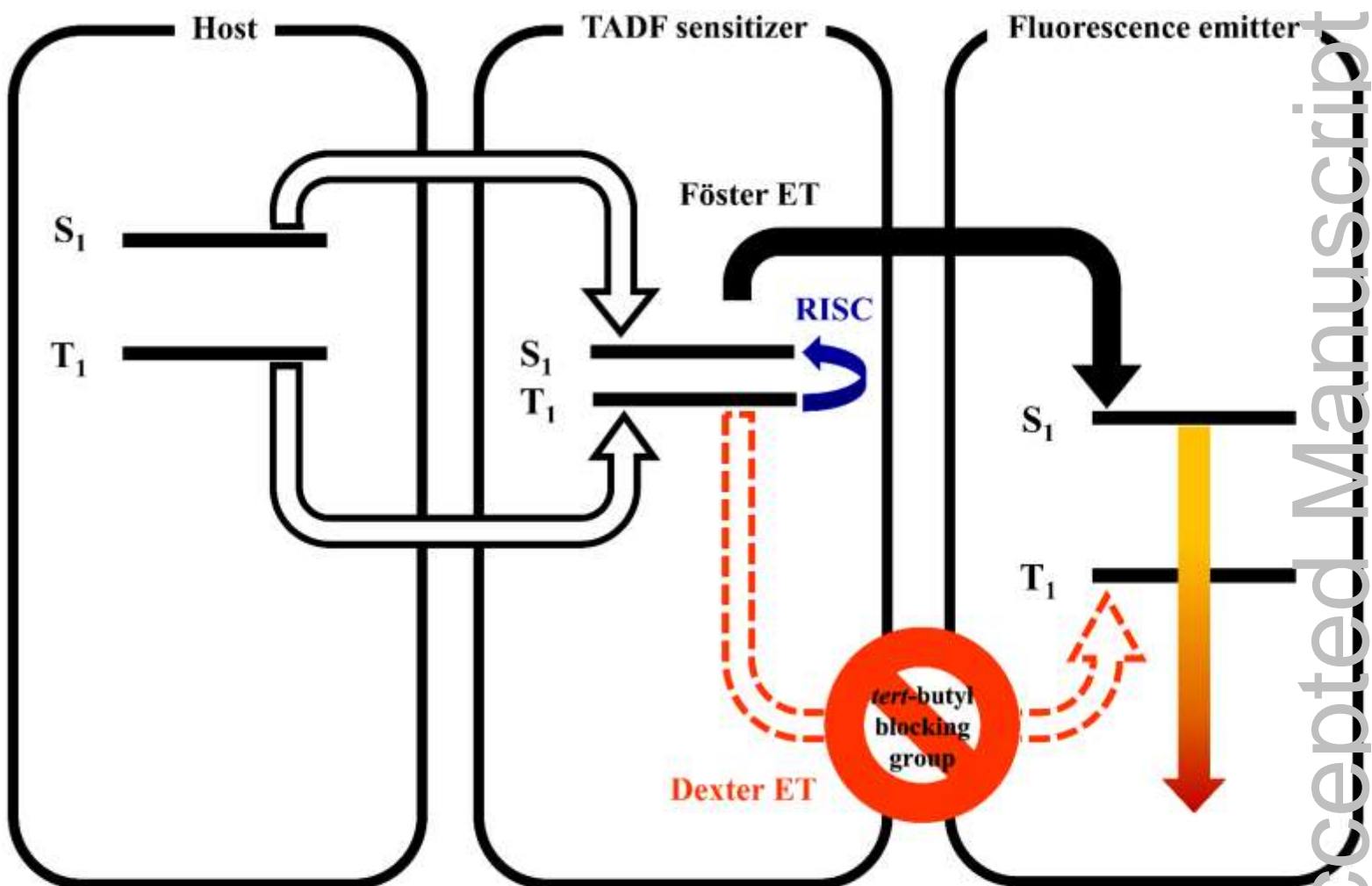
To be cited as: *Chem. Eur. J.* 10.1002/chem.202004042

Link to VoR: <https://doi.org/10.1002/chem.202004042>

WILEY-VCH

Table-of-content

Efficient TADF sensitizer: Three TADF materials having fast reverse intersystem crossing rate were developed for TADF sensitizer. Among these, two TADF materials include *tert*-butyl blocking group to manage Dexter energy transfer. The TADF sensitized fluorescent devices with blocking groups showed high maximum external quantum efficiencies. In addition, the device operational lifetime was extended by adding blocking groups.



Design approach of lifetime extending thermally activated delayed fluorescence sensitizers for highly efficient fluorescence devices

Sung Joon Yoon, Ji Han Kim, Won Jae Chung, Jun Yeob Lee*

School of Chemical Engineering, Sungkyunkwan University, 2066, Seobu-ro, Jangan-gu, Suwon-si, Gyeonggi-do, 440-746, Republic of Korea

* Corresponding author
E-mail: leej17@skku.edu

Abstract

In this work, a design approach of three thermally activated delayed fluorescence (TADF) emitters to extend the device lifetime of the TADF sensitized fluorescent devices was studied. Three TADF materials, 5-(4,6-bis(4-(*tert*-butyl)phenyl)-1,3,5-triazin-2-yl)-2-(10,15-diphenyl-10,15-dihydro-5*H*-diindolo[3,2-*a*:3',2'-*c*]carbazol-5-yl)benzotrile (**tTCNTruX**), 4-(3-cyano-4-(10,15-diphenyl-10,15-dihydro-5*H*-diindolo[3,2-*a*:3',2'-*c*]carbazol-5-yl)phenyl)-2,6-diphenylpyrimidine-5-carbonitrile (**PCNTruX**) and 4-(4-(10,15-bis(4-(*tert*-butyl)phenyl)-10,15-dihydro-5*H*-diindolo[3,2-*a*:3',2'-*c*]carbazol-5-yl)-3-cyanophenyl)-2,6-diphenylpyrimidine-5-carbonitrile (**PCNtTruX**), were synthesized as the sensitizers of the TADF sensitized fluorescent organic light-emitting diodes. The two **tTCNTruX** and **PCNtTruX** TADF emitters were designed to have Dexter energy transfer managing blocking groups either in the donor or acceptor unit of the donor-acceptor type TADF sensitizer. The TADF materials showed small singlet-triplet energy splitting and high reverse intersystem crossing (RISC) rate for effective sensitization of the fluorescent emission of the fluorescent emitter. The **tTCNTruX** and **PCNtTruX** sensitized fluorescent devices showed maximum external quantum efficiencies (EQEs) of 17.7% and 11.5% in the yellow and red devices,

respectively, which were higher than those of the TADF sensitized devices with the corresponding TADF sensitizer without the blocking group. Moreover, the device lifetime was also extended by employing the **tTCNTruX** and **PCNtTruX** sensitizers. This work demonstrated that the **tTCNTruX** and **PCNtTruX** sensitizers are effective to upgrade the maximum EQE and device lifetime of the TADF sensitized fluorescent devices.

Key words : Organic light-emitting diodes, TADF, TADF sensitizer, blocking group

Introduction

Fluorescence emitters have been the first generation light-emitting materials of organic light-emitting diodes (OLEDs) showing long lifetime and high color purity. However, fluorescence emitters can achieve theoretical internal quantum efficiency (IQE) of only 25% according to the spin statistics, which a big hurdle of them. To tackle the low efficiency of the fluorescence emitters, thermally activated delayed fluorescence (TADF) emitters enabling theoretical IQE of 100% were developed recently [1-4]. The basic principle of TADF is the triplet exciton up-conversion from triplet excited state to singlet excited state through the reverse intersystem crossing (RISC) due to small singlet-triplet energy splitting (ΔE_{ST}). To get the small ΔE_{ST} , the orbital overlap between the highest occupied molecular orbital (HOMO) and lowest unoccupied molecular orbital (LUMO) should be minimized. Therefore, the TADF materials are generally designed to have electron acceptor and electron donor moieties to separate the HOMO and LUMO [1]. However, this design strategy involves structure relaxation that results in increased Stokes shift and broad full width at half maximum (FWHM) harmful to the color purity [5, 6]. Moreover, the TADF devices suffer from short device lifetime compared to the fluorescence devices.

In 2014, Adachi group developed the so-called hyperfluorescence (TADF sensitized fluorescence) system combining TADF sensitizer and fluorescence emitter to overcome the disadvantages of the TADF and fluorescence [7]. In the hyperfluorescence system, the TADF sensitizer harvests triplet excitons to singlet excitons by RISC process and the up-converted singlet excitons transfer emission energy to the fluorescence emitter by Förster resonance energy transfer (FRET) process. The hyperfluorescence device can have advantage over the TADF device for operation lifetime because of accelerated RISC process reducing the triplet exciton lifetime in the emission process [8]. Additionally, the color purity is improved since the emission comes from the fluorescence materials. However, the triplet exciton energy of the TADF sensitizer is also transferred to the fluorescence emitter by Dexter energy transfer (DET) which is critical to the device performances. Therefore, fast RISC of the TADF sensitizer and suppression of DET from the TADF sensitizer to the fluorescence emitter are needed to show high efficiency. To hinder the DET process, interrupting orbital overlap by increasing the distance between the TADF sensitizer and fluorescence emitter is efficient [9, 10]. In particular, the addition of blocking groups to the TADF sensitizer can reduce the intermolecular interaction and inhibit the DET process.

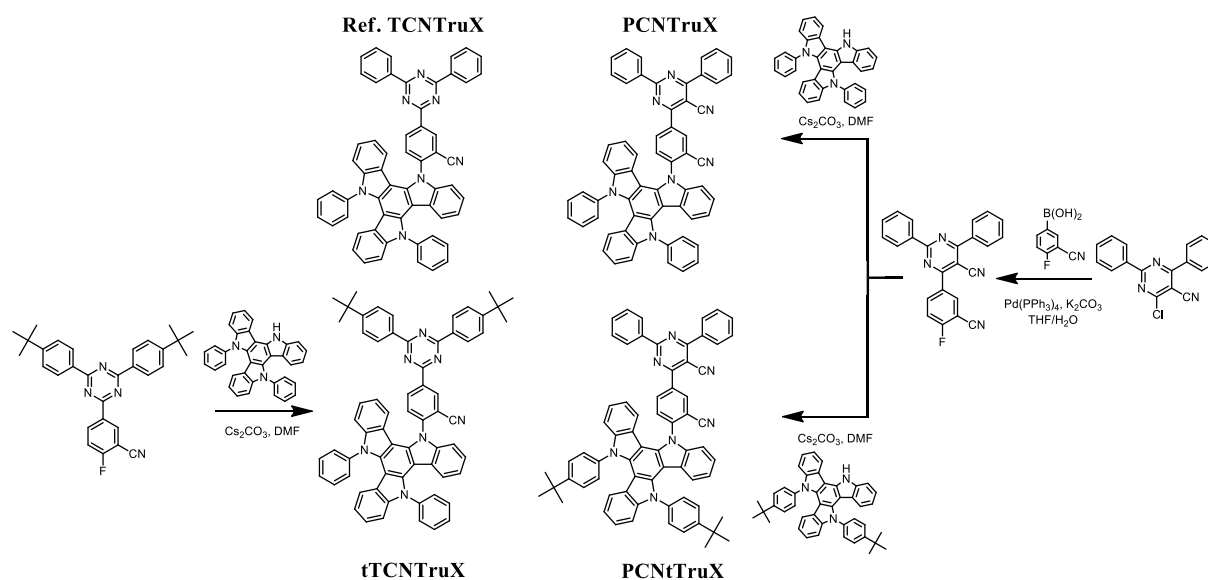
In this work, we developed 5-(4,6-bis(4-(*tert*-butyl)phenyl)-1,3,5-triazin-2-yl)-2-(10,15-diphenyl-10,15-dihydro-5*H*-diindolo[3,2-*a*:3',2'-*c*]carbazol-5-yl)benzotrile (**tTCNTruX**), 4-(3-cyano-4-(10,15-diphenyl-10,15-dihydro-5*H*-diindolo[3,2-*a*:3',2'-*c*]carbazol-5-yl)phenyl)-2,6-diphenylpyrimidine-5-carbonitrile (**PCNTruX**) and 4-(4-(10,15-bis(4-(*tert*-butyl)phenyl)-10,15-dihydro-5*H*-diindolo[3,2-*a*:3',2'-*c*]carbazol-5-yl)-3-cyanophenyl)-2,6-diphenylpyrimidine-5-carbonitrile (**PCNtTruX**) as TADF sensitizers in yellow and red hyperfluorescence devices. The **tTCNTruX** was compared with 5-(4,6-diphenyl-1,3,5-triazin-2-yl)-2-(10,15-diphenyl-10,15-dihydro-5*H*-diindolo[3,2-*a*:3',2'-*c*]carbazol-5-yl)benzotrile

(**TCNTruX**) in the yellow hyperfluorescence OLEDs doped with 2,8-di-*tert*-butyl-5,11-bis(4-*tert*-butylphenyl)-6,12-diphenyltetracene (TBRb) [11]. Whereas, the **PCNTruX** and **PCNtTruX** were used as TADF sensitizers in the red hyperfluorescence OLEDs doped with 5,10,15,20-tetraphenylbisbenz[5,6]indeno[1,2,3-*cd*:1',2',3'-*lm*]perylene (DBP). The **tTCNTruX** and **PCNtTruX** sensitized hyperfluorescence devices showed maximum external quantum efficiencies (EQEs) of 17.7% and 11.5% in the yellow and red devices, respectively, which were higher than those of the **TCNTruX** and **PCNTruX** sensitized devices. Additionally, the device lifetime of the hyperfluorescence devices was extended by using the TADF sensitizers with the blocking groups.

Results and discussion

The main design concept of the TADF sensitizers is to add *tert*-butyl units to the donor or acceptor part of the TADF molecules to suppress the DET process and enhance device operational lifetime in the yellow and red hyperfluorescence system. The basic donor moiety of the molecular design was 5,10-diphenyl-10,15-dihydro-5*H*-diindolo[3,2-*a*:3',2'-*c*]carbazole (TruX) which causes a large torsion angle by connection with a phenyl linker. In previous work, 3-(4,6-diphenyl-1,3,5-triazin-2-yl)benzotrile (TCN) and 4-(3-cyanophenyl)-2,6-diphenylpyrimidine-5-carbonitrile (PCN) were integrated with the TruX unit. The TCN unit was modified with *tert*-butyl blocking groups, offering the **tTCNTruX** TADF material. The acceptor of the red TADF sensitizer was the PCN moiety which has stronger electron deficiency than the TCN moiety because of additional CN group. Instead of the *tert*-butyl modification of the acceptor unit, the TruX donor unit was protected with the *tert*-butyl blocking group to synthesis **PCNtTruX**. Two TADF materials, **tTCNTruX** and **PCNtTruX**, were designed to

identify the influence of blocking groups on the energy transfer, efficiency and device lifetime of the hyperfluorescence system. The synthesis of the TADF materials is shown in Scheme 1 and the scheme for the intermediate materials is presented in the supporting Scheme S1. The details of the reaction conditions and reagents are presented in experimental part of the supporting information. The final products purified by column chromatography and sublimation were confirmed through nuclear magnetic resonance (NMR) and gas chromatography high resolution mass spectrometry (GC-HRMS).



Scheme 1. Synthesis scheme of **tTCNTruX**, **PCNTruX** and **PCNtTruX**, and chemical structure of **TCNTruX**.

Through Gaussian 16 based on the B3LYP 6-31G basis set, the orbital distribution and optimized geometry of the three TADF materials in the ground state were determined by

electronic calculations. Figure 1 shows the orbital distribution of the HOMO/LUMO and the calculated photophysical properties of the **tTCNTruX**, **PCNTruX** and **PCNtTruX**. The optimized structure of the TADF materials in ground state is shown in Figure S1. As a result of the simulation, the dihedral angles between the acceptor and donor moieties were 72.5°, 76.9° and 65.6° in the **tTCNTruX**, **PCNTruX** and **PCNtTruX** owing to the steric hindrance of the TruX unit. Due to the twisted structure between the donor and acceptor units, the HOMO and LUMO distributions showed almost separated molecular orbitals. The HOMO was commonly localized on the TruX electron donating unit, and the LUMO was dispersed over the TCN and PCN electron withdrawing unit. The *tert*-butyl groups had little effect on the HOMO and LUMO orbital pictures. The calculated HOMO/LUMO levels of the **tTCNTruX**, **PCNTruX** and **PCNtTruX** were -4.92/-2.12, -4.85/-2.42 and -4.87/2.41 eV, respectively. The LUMO level was estimated to be deeper in the **PCNTruX** and **PCNtTruX** due to the strongly electron deficient PCN moiety by the pyrimidine and an additional CN unit. The calculated singlet/triplet energies of **tTCNTruX**, **PCNTruX** and **PCNtTruX** were 2.37/2.33 eV, 2.06/2.05 eV and 2.11/2.10 eV, respectively. The ΔE_{ST} values were less than 0.04 eV, which was small enough to trigger RISC process. The *tert*-butyl addition had little effect on the energy level and emission energy of the TADF materials. The calculated oscillator strength was higher in the **tTCNTruX** than the **PCNtTruX**, indicating that **tTCNTruX** may show higher PLQY value than **PCNtTruX**.

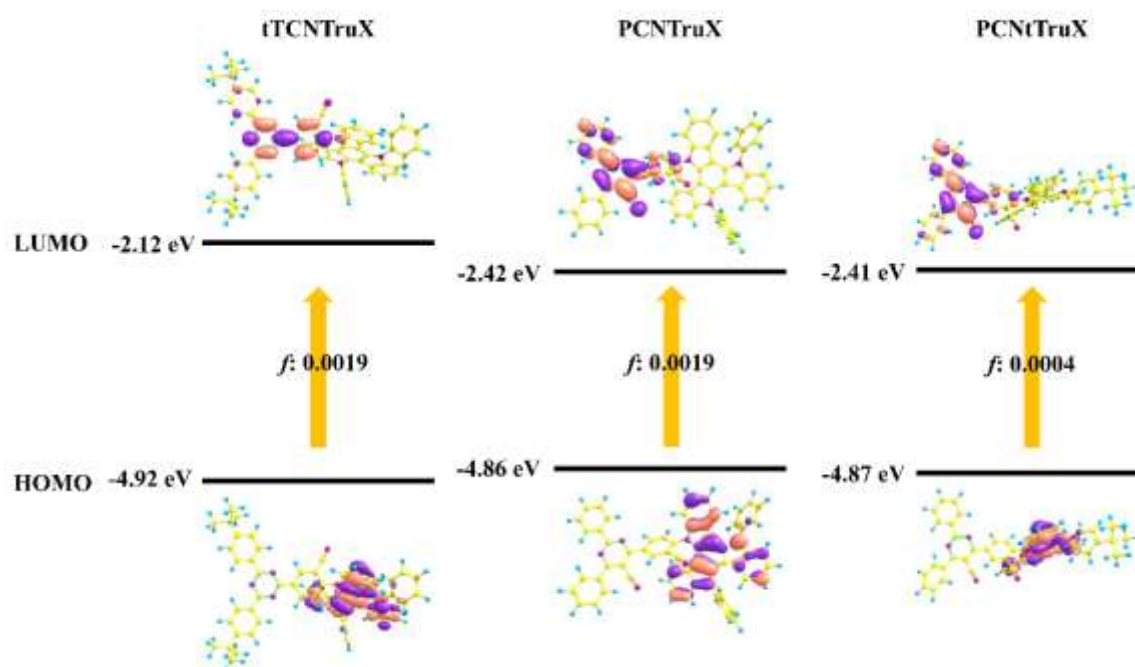


Figure 1. Calculated HOMO and LUMO distributions, and energy levels of **tTCNTruX**, **PCNTruX** and **PCNtTruX**.

The ultraviolet-visible (UV-Vis) absorption and photoluminescence (PL) measurements were used to determine the photophysical properties of the **tTCNTruX**, **PCNTruX** and **PCNtTruX** in dilute tetrahydrofuran (THF) solution. Figure 2 shows UV-Vis absorption and PL spectra of the three TADF materials. In the UV-Vis absorption spectra, the three materials showed similar spectra because their backbone structure was analogous. The only difference was the slight red shift of the absorption spectra in the PCN derived materials. The broad absorption below 500 nm region demonstrates the intramolecular charge transfer (ICT) transition from the TruX donor to the acceptor unit. The molar extinction coefficient (ϵ) of the **tTCNTruX** material was relatively larger ($6.6 \times 10^3 \text{ M}^{-1} \text{ cm}^{-1}$) than that of the others ($4.5 \times 10^3 \text{ M}^{-1} \text{ cm}^{-1}$), indicating the strong absorption by large HOMO/LUMO overlap in **tTCNTruX**. The onset values of the UV-

Vis absorption were 476 nm, 482 nm and 484 nm in the **tTCNTruX**, **PCNTruX** and **PCNtTruX**, respectively. The singlet and triplet energy values of the TADF materials were measured by fluorescent and phosphorescent PL measurements in dilute THF solution at 77 K without and with 2.0 ms delay time. The singlet/triplet energy values of the **tTCNTruX**, **PCNTruX** and **PCNtTruX** were 2.68/2.65, 2.66/2.67 and 2.64/2.68 eV, respectively. The peak wavelengths of the fluorescence emission of the **tTCNTruX**, **PCNTruX** and **PCNtTruX** were 532, 544 and 547 nm, respectively. Two materials, **PCNTruX** and **PCNtTruX**, showed long emission wavelength because of the strong PCN acceptor moiety. The measured ΔE_{ST} values were small enough to show TADF characteristics. The negative ΔE_{ST} of the **PCNTruX** and **PCNtTruX** might be due to the local triplet emission of the emitters.

Cyclic voltammetry (CV) was used to estimate the HOMO and LUMO energy levels of the TADF materials. The CV data of three TADF materials are shown in Figure S2. The HOMO/LUMO energy levels of **tTCNTruX**, **PCNTruX** and **PCNtTruX** were -5.78/-3.53, -5.83/-3.64 and -5.83/-3.63 eV, respectively, which agreed with the tendency of the molecular simulation. As the **PCNTruX** and **PCNtTruX** contain the strongly electron deficient PCN unit, the LUMO energy level was deep.

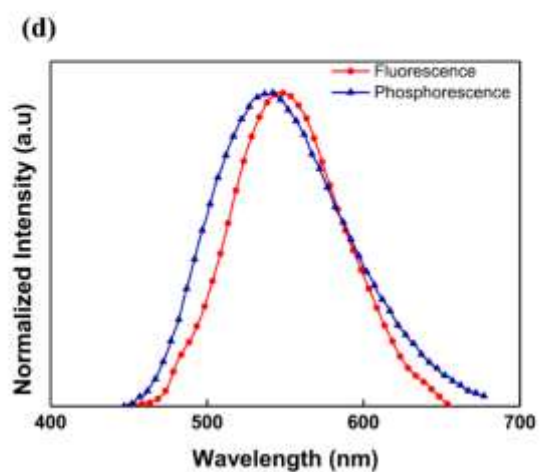
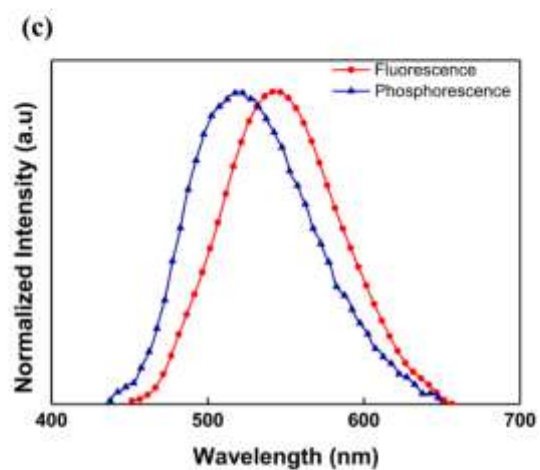
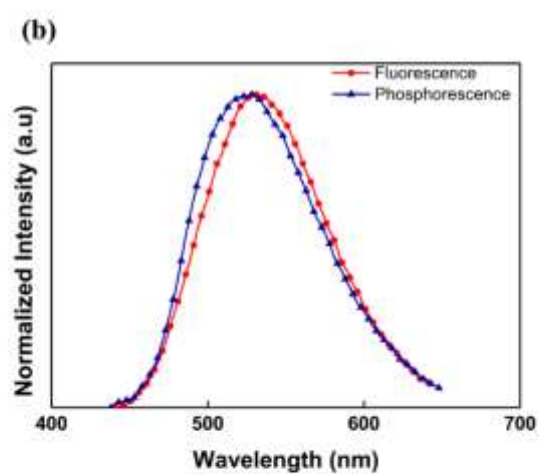
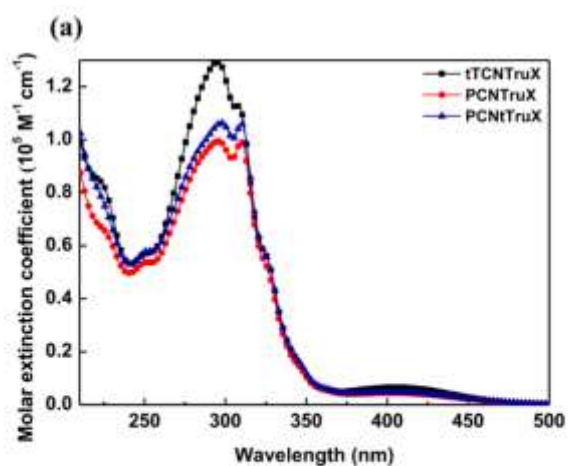


Figure 2. UV-Vis absorption spectra (a) and fluorescence/phosphorescence emission spectra of the (b) **tTCNTruX** (c) **PCNTruX** and (d) **PCNtTruX**.

The absolute PL quantum yields (PLQYs) of **tTCNTruX** and **PCNtTruX** were measured to identify PL efficiency of the TADF materials. The TCN derived **tTCNTruX** were analyzed in the 9-(3'-(4,6-diphenyl-1,3,5-triazin-2-yl)-[1,1'-biphenyl]-3-yl)-9*H*-carbazole (CzTrz) host at 20 wt% doping concentration, and the PCN derived **PCNtTruX** were investigated in the 12,12'-(6-phenyl-1,3,5-triazine-2,4-diyl)bis(11-phenyl-11,12-dihydroindolo[2,3-*a*]carbazole) (PBICT)/4-(3-(triphenyl-2-yl)phenyl)dibenzo[*b,d*]thiophene (DBTTP1) mixed host (70/30) at 10 wt% doping concentration [12]. The PLQY of the **TCNTruX** and **PCNTruX** was also measured for comparison. The PLQY value of **TCNTruX/tTCNTruX** under nitrogen was measured to be 47.9/65.2%, and that of **PCNTruX/PCNtTruX** was 47.1/45.0%. The **TCNTruX** and **PCNTruX** showed similar PLQY values, whereas the **tTCNTruX** exhibited higher PLQY than **PCNtTruX**. The *tert*-butyl modification increased the PLQY of the **tTCNTruX**. The reason might be the difference of CT character by the *tert*-butyl modification. The *tert*-butyl groups on the acceptor moiety in **tTCNTruX** enhance the HOMO/LUMO overlap by decreasing the CT character through the weakened acceptor character. The enhancement of HOMO/LUMO overlap leads to relatively high PLQY value. Whereas, the **PCNtTruX** which has *tert*-butyl groups on the donor moiety tends to have opposite effect [13]. Additionally, the *tert*-butyl group of **tTCNTruX** can prevent intermolecular interaction between planar acceptors for suppressed exciton quenching, enhancing the PLQY.

The transient PL (TRPL) was used to measure prompt fluorescence decay time (τ_p) and delayed fluorescence decay time (τ_d) to study photophysical dynamics of the emitters. The

TRPL decays of the TCN derivatives and PCN derivatives were almost the same, indicating that *tert*-butyl groups did not affect the decay time. The τ_p values were 75.8/76.3 ns in **TCNTruX/tTCNTruX**, and 102.4/126.5 ns in **PCNTruX/PCNtTruX**, respectively. The τ_d values were 1.08/1.28 μ s in **TCNTruX/tTCNTruX**, and 1.06/1.00 μ s in **PCNTruX/PCNtTruX**. The prompt and delayed fluorescence curves of TRPL are shown in Figure 3. The intersystem crossing (ISC), RISC, radiative (k_r^S) and non-radiative (k_{nr}^T) rate constants of the TADF emitters were calculated by PLQY and TRPL measurement values using the method reported in the literature [14]. Table 1 shows the summary of the PLQY, TRPL data and rate constants of the four TADF materials. The RISC rate constants ($\times 10^5 \text{ s}^{-1}$) of the four TADF materials were calculated to be over 13.6, and non-radiative rate constants ($\times 10^5 \text{ s}^{-1}$) were less than 6.94 indicating that the four TADF materials are suitable for the TADF sensitizer in the hyperfluorescence devices.

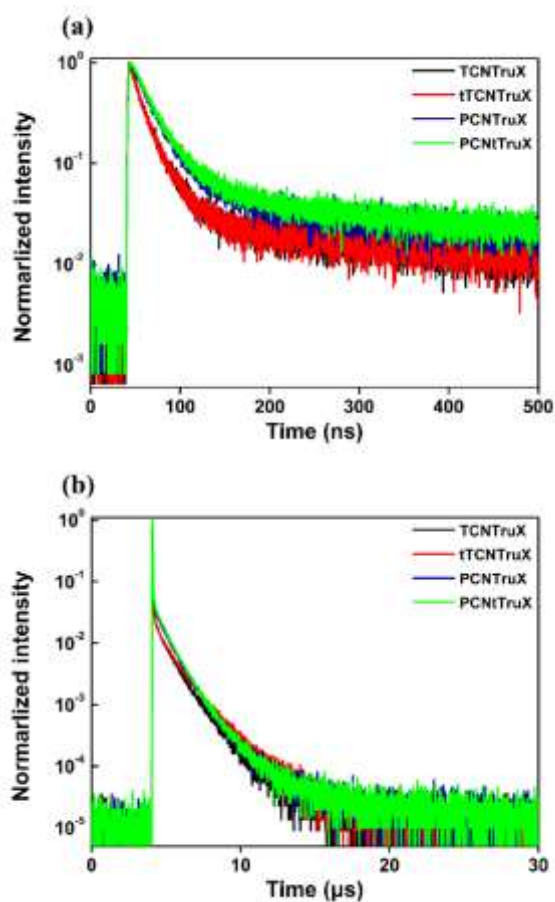


Figure 3. Transient PL graphs of (a) Prompt and (b) Delay fluorescence of **tTCNTruX**, **PCNTruX**, **PCNtTruX** and reference material **TCNTruX**.

Table 1. The PLQY, transient PL data and calculated rate constants of **tTCNTruX**, **PCNTruX**, **PCNtTruX** and reference material **TCNTruX**.

	PLQY			τ_p [ns]	τ_d [μs]	k_{ISC} [$\times 10^6 \text{ s}^{-1}$]	k_{RISC} [$\times 10^5 \text{ s}^{-1}$]	k_r^S [$\times 10^6 \text{ s}^{-1}$]	k_{nr}^T [$\times 10^5 \text{ s}^{-1}$]
	Φ	$\Phi_F^{(a)}$	$\Phi_{TADF}^{(b)}$						
	[%]	[%]	[%]						
TCNTruX	47.9	21.2	26.7	75.8	1.08	10.4	14.8	2.80	6.14
tTCNTruX	65.2	29.3	35.9	76.3	1.28	9.27	13.6	3.84	3.86

PCNTruX	47.1	21.4	25.7	102.4	1.06	7.67	14.4	2.09	6.35
PCNtTruX	45.0	21.0	24.0	126.5	1.00	6.24	14.4	1.66	6.94

(a) Absolute PL quantum yield measured under an oxygen atmosphere (b) Absolute PL quantum yield of the TADF component

In addition, the TBRb and DBP fluorescence dopants were additionally doped at 0.5 wt% doping concentration to the TADF materials to verify the photophysical dynamics in hyperfluorescence system by PLQY and TRPL measurements. The TRPL graphs of the four TADF emitters with the fluorescence dopants are shown in Figure 4. The delayed fluorescence decay time of the TADF materials was shortened by the doping of the fluorescent emitters. The fast FRET process from the TADF sensitizer to the fluorescent dopant accelerates the RISC process of the TADF materials, shortening the delayed decay time. The PLQY values of **TCNTruX:TBRb/tTCNTruX:TBRb** and **PCNTruX:DBP/PCNtTruX:DBP** were 72.8/82.8% and 76.4/75.7%, respectively. The PLQY was increased by the doping of the fluorescence dopants because the emission energy of the non-radiative excitons were transferred to the fluorescent dopant.

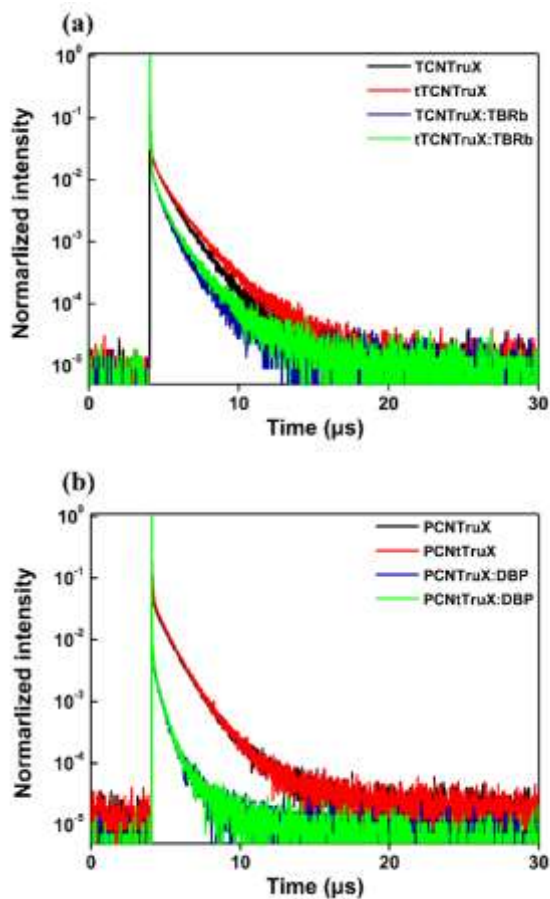


Figure 4. Transient PL graphs of the (a) **TCNTTruX/tTCNTTruX** without or with TBRb and (b) **PCNTTruX/PCNtTruX** without or with DBP.

To verify the performance of the TADF materials as the TADF emitters and sensitizers, the electroluminescence (EL) devices were fabricated with the TADF materials and fluorescent emitters. The common structure of the EL devices was indium tin oxide (ITO) (50 nm)/ N1,N1-(biphenyl-4,4-diyl)bis(N1-phenyl-N4,N4-di-m-tolylbenzene-1,4-diamine) (DNTPD) (60 nm)/ N,N,N',N'-tetra[(1,1'-biphenyl)-4-yl]-(1,1'-biphenyl)-4,4'-diamine (BPBPA) (20 nm)/ 9,9-dimethyl-10-(9-phenyl-9H-carbazol3-yl)-9,10-dihydroacridine (PCZAC) (10 nm)/ emitting layer (30 nm)/ 2,8-bis(4,6-diphenyl-1,3,5-triazin-2-yl)dibenzo[*b,d*]furan (DBFTrz) (5 nm)/ 2-

[4-(9,10-di-naphthalen-2-yl-anthracene-2-yl)-phenyl]-1-phenyl-1H-benzimidazole (ZADN) (30 nm)/ LiF (1.5 nm)/ Al (200 nm). The 20 wt% **tTCNTruX** or **TCNTruX** doped emitting layer with and without the 0.5 wt% doped TBRb yellow fluorescence dopant was used in the yellow devices. The CzTrz host material was commonly applied in the yellow TADF and hyperfluorescence device. Similarly, the 10 wt% doped **PCNTruX** or **PCNtTruX** TADF materials were used as the emitting layer in the TADF device and that of 20 wt% TADF materials and 0.5 wt% DBP red fluorescence dopant was employed in the red devices. The PBICT and DBTTP1 mixed host (70:30) was commonly used in the red TADF and hyperfluorescence devices. Figure 5 shows the energy level diagram of the devices.

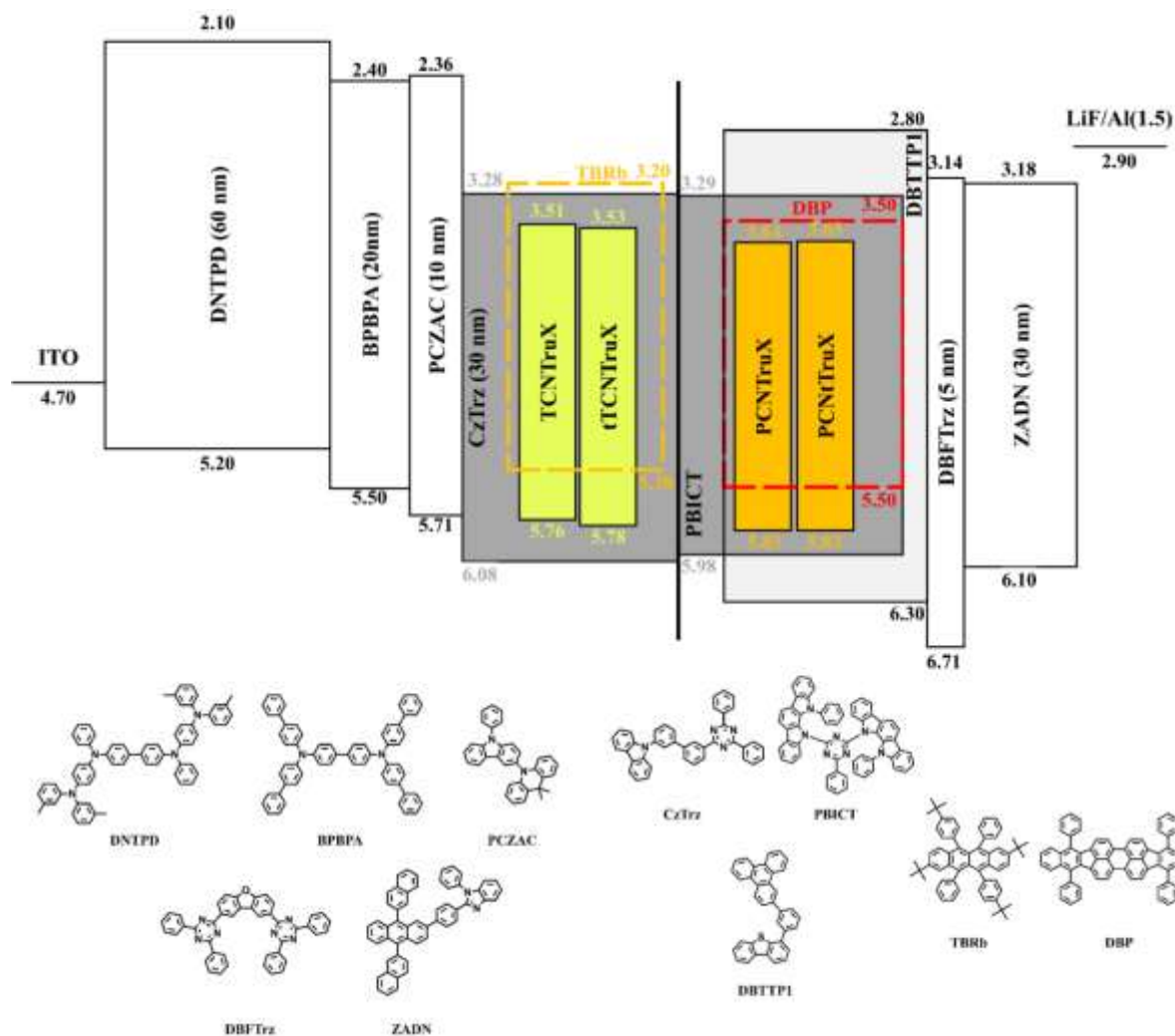


Figure 5. The energy level diagram of the **TCNTruX**, **tTCNTruX**, **PCNTruX** and **PCNtTruX** devices.

The current density (J)-voltage (V)-luminance (L) data, EQE- L plots and EL spectra of the TADF devices and hyperfluorescence devices are shown in Figure 6 and Figure 7. The J values of the **TCNTruX** and **tTCNTruX** devices were analogous, indicating that the *tert*-butyl blocking group has little effect on the carrier transport properties of the emitters considering the similar HOMO and LUMO levels of the two TADF materials. The **PCNTruX** and **PCNtTruX** devices followed the same trend. The maximum EQEs of the **TCNTruX** and

tTCNTruX devices were 15.3 and 18.4 % at 20 wt% doping concentration with efficiency drop of only 0.6 and 0.5% at 1,000 cd m⁻², respectively. The EQE was rather degraded in the **PCNTruX** (10.2%) and **PCNtTruX** (9.3%) devices by the non-radiative loss according to the energy gap law. The maximum EQEs of the four TADF materials followed the trend of the PLQY values. The EQE reduction at 1,000 cd m⁻² was only 2.2%. Generally, the TADF materials have RISC rate of about 10⁵ s⁻¹, but the four TADF materials achieved 10 times higher RISC rate than other TADF materials. Accordingly, the up-conversion was facilitated, which suppressed the EQE roll-off of the TADF devices.

The EL peak wavelengths of the **TCNTruX**, **tTCNTruX**, **PCNTruX** and **PCNtTruX** devices were 554, 548, 563 and 565 nm, respectively. The **PCNTruX** and **PCNtTruX** devices emitted relatively at long wavelengths as shown in the PL spectra of the TADF materials. The short wavelength shift of the EL spectrum of **tTCNTruX** relative to that of **TCNTruX** is due to the slightly weakened acceptor strength by the electron donating character of the *tert*-butyl unit. The Commission International de l'Eclairage (CIE) coordinates of the **TCNTruX**, **tTCNTruX**, **PCNTruX** and **PCNtTruX** devices were (0.42, 0.55), (0.40, 0.56), (0.46, 0.52) and (0.47, 0.52), respectively.

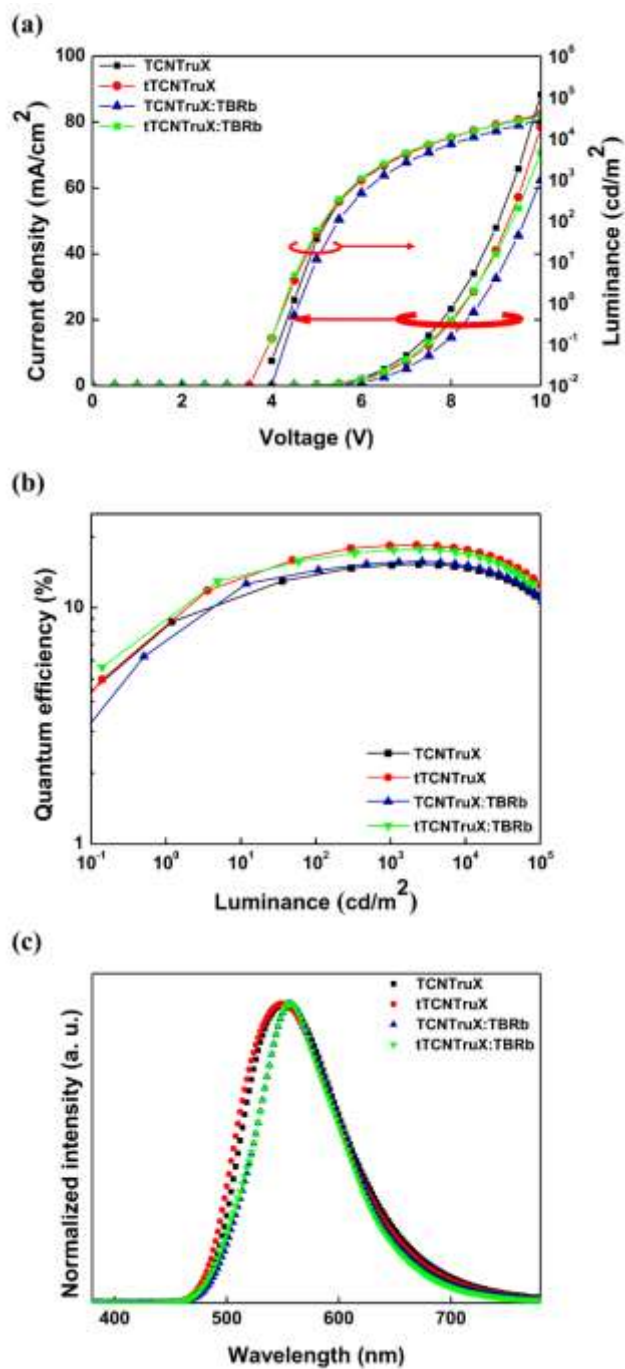


Figure 6. (a) The *J-V-L* data, (b) EQE-*L* plots and (c) EL spectrum of the TCNTTruX and tTCNTTruX TADF devices and sensitized TBRb devices.

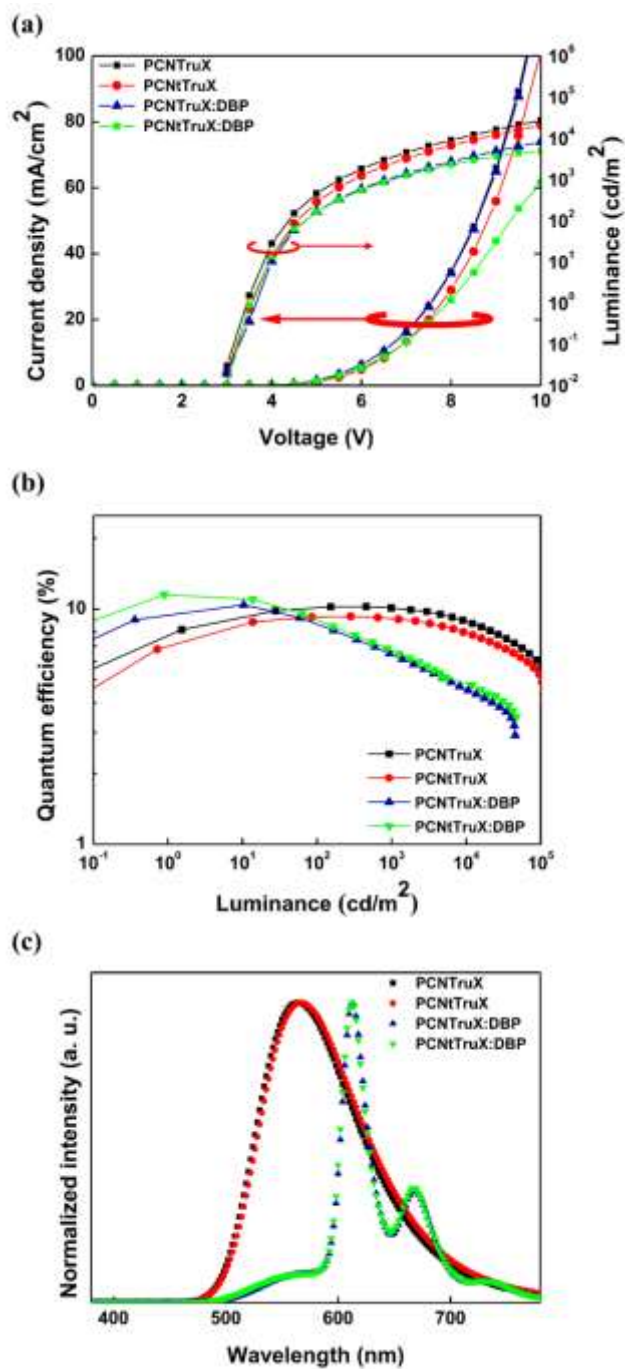


Figure 7. (a) The $J-V-L$ data, (b) EQE- L plots and (c) EL spectrum of the **PCNTTruX** and **PCNTTruX** TADF devices and sensitized DBP devices.

In the hyperfluorescence devices, the maximum EQEs of the **TCNTTruX** and **tTCNTTruX**

devices with the TBRb yellow dopant were 15.7 and 17.7%, while those of the **PCNTruX** and **PCNtTruX** devices with the DBP red dopant were 10.4 and 11.5%, respectively. As a result, the hyperfluorescence devices with the *tert*-butyl modified TADF materials showed improved EQE. In the TCN derivatives, the EQE of the hyperfluorescence devices followed the EQE tendency of the TADF devices. Whereas, in the red hyperfluorescence devices, the **PCNtTruX** device showed higher EQE than the **PCNTruX** device in spite of low EQE in the TADF device.

This result can be interpreted based on the energy transfer process from the TADF materials to the fluorescent dopant. In general, both FRET and DET contribute to the energy transfer process in the hyperfluorescence devices. The FRET process is desirable for high EQE, but the DET process has to be avoided because it is an exciton loss mechanism. Therefore, the DET has to be managed by molecular engineering. In the **PCNtTruX** material, the *tert*-butyl was added as the bulky blocking group and it can control the DET from it to the DBP dopant. The suppression of the DET process can up-convert more triplet excitons into singlet excitons, which can increase the EQE of the hyperfluorescence devices. To prove the DET suppressing role of the *tert*-butyl blocking groups, PLQY dependence of the **PCNTruX** and **PCNtTruX** emitting layer was measured by changing the doping concentration of the TADF compound and DBP. Table S1 and Table S2 show the PLQY values of hyperfluorescence emitting layer. When the *tert*-butyl group was absent, the PLQY was reduced by increasing the TADF and DBP doping concentration because of DET. However, the PLQY remains almost constant irrespective of the TADF and DBP doping concentration because the DET is suppressed. In the case of the **tTCNTruX**, the *tert*-butyl unit suppressed quenching mechanisms of the TADF emission and improve radiative transition probability as shown in the PLQY, which increased the EQE of the hyperfluorescence devices. Therefore, the device performances of the hyperfluorescence device agreed with the trend of those of the TADF device.

The EL spectra of the hyperfluorescence devices represent that the EL emission is originated partially from the TADF materials and partially from the fluorescence dopant. The CIE coordinates of the **TCNTruX** and **tTCNTruX** sensitized TBRb devices were (0.43, 0.54) and (0.43, 0.55), respectively, and that of the **PCNTruX** and **PCNtTruX** sensitized DBP devices was (0.63, 0.37). Table 2 and Table 3 show the EL performances of the TADF and hyperfluorescence devices.

Table 2. EL performance of the **TCNTruX** and **tTCNTruX** TADF devices and hyperfluorescence devices.

Device ^(a)	V _d ^(b) [V]	V _{on} ^(c) [V]	External Quantum efficiency [%]		Power efficiency [lm/W]		Current efficiency [cd/A]		CIE ^(d) (x, y)	Device lifetime ^(e) [h]
			1000cd/m ²	Max	1000cd/m ²	Max	1000cd/m ²	Max		
TCNTruX (20%)	6.0	4.4	15.2	15.3	25.1	26.5	47.8	48.1	(0.42, 0.55)	393
tTCNTruX (20%)	6.0	4.1	18.3	18.4	30.5	32.5	58.3	58.5	(0.40, 0.56)	734
TCNTruX:TBRb (20%:0.5%)	6.3	4.5	15.5	15.7	25.0	26.8	50.2	50.7	(0.43, 0.54)	392
tTCNTruX:TBRb (20%:0.5%)	5.9	4.1	17.5	17.7	30.5	32.5	57.6	58.1	(0.43, 0.55)	593

(a) ITO/DNTPD/BPBPA/PCZAC/**emitter**:CzTrz/DBFTzr/ZADN/LiF/Al (b) V_d: driving voltage at 1000 cd m⁻² (c) V_{on}: turn on voltage (driving voltage at 1 cd m⁻²) (d) At 1000 cd m⁻² (e) LT90 at 1000 cd m⁻²

Table 3. EL performance of the **PCNTruX** and **PCNtTruX** TADF devices and hyperfluorescence devices.

Device ^(a)	V _d ^(b) [V]	V _{on} ^(c) [V]	External Quantum efficiency [%]		Power efficiency [lm/W]		Current efficiency [cd/A]		CIE ^(d) (x, y)	Device lifetime ^(e) [h]
			1000cd/m ²	Max	1000cd/m ²	Max	1000cd/m ²	Max		

PCNTruX (10%)	5.5	3.3	10.1	10.2	16.8	22.1	29.4	29.7	(0.46, 0.52)	2360
PCNtTruX (10%)	5.8	3.5	9.1	9.3	14.0	19.1	25.7	26.1	(0.47, 0.52)	1685
PCNTruX:DBP (20%:0.5%)	6.6	3.5	6.4	10.4	4.3	10.3	9.0	13.1	(0.63, 0.37)	599
PCNtTruX:DBP (20%:0.5%)	6.7	3.5	6.7	11.5	4.6	13.1	9.7	14.6	(0.63, 0.37)	919

(a) ITO/DNTPD/BPBPA/PCZAC/**emitter**:PBICT:DBTTP1/DBFTTrz/ZADN/LiF/Al (b) V_d : driving voltage at 1000 cd m⁻²
(c) V_{on} : turn on voltage (driving voltage at 1 cd m⁻²) (d) At 1000 cd m⁻² (e) LT90 at 1000 cd m⁻²

The device operational lifetime of the TADF and hyperfluorescence devices was measured at 1,000 cd m⁻² at a constant current operation mode. Figure 8 shows the device lifetime curves of the TADF and hyperfluorescence devices of **TCNTruX**, **tTCNTruX**, **PCNTruX** and **PCNtTruX**. In the case of TCN derivatives, **tTCNTruX** achieved long device lifetime compared to **TCNTruX** in both TADF and hyperfluorescence devices. The **TCNTruX** and **tTCNTruX** sensitized TBRb devices showed the device lifetime of 392 and 593 h up to 90% of the initial luminance (LT90) at 1,000 cd m⁻², respectively. Compare with 4CzIPN-Me:TBRb hyperfluorescence device in previous work, the device lifetime was extended by more than 2 times [15]. However, in the case of the PCN derivatives, the **PCNtTruX** with the *tert*-butyl blocking groups achieved shorter device lifetime in the TADF device, but longer lifetime in the hyperfluorescence device than the **PCNTruX** device. The opposite trend of the device lifetime in the TADF and hyperfluorescence devices might be due to the DET control in the hyperfluorescence devices. As the DET is an exciton loss mechanism, the DET process would accelerate the efficiency loss of the hyperfluorescence device corresponding to the lifetime degradation. Therefore, the DET management is helpful to the device lifetime of the

hyperfluorescence device, increasing the device lifetime of the **PCNtTruX** device. The **PCNTruX** and **PCNtTruX** sensitized DBP devices showed the lifetime of 599 and 919 h (LT90) at 1,000 cd m⁻², respectively. This shorter device lifetime of the **PCNtTruX** TADF device may be due to long delayed fluorescence lifetime and low EQE of the PCNtTruX emitter relative to that of PCNTruX in spite of DET suppressing function of the tert-butyl units. The relatively short device lifetime of the red hyperfluorescence device compared to the TADF device is caused by red shift of the emission spectrum. As the device lifetime was measured at the same luminance, the red hyperfluorescence device shows shorter device lifetime than the yellow TADF device.

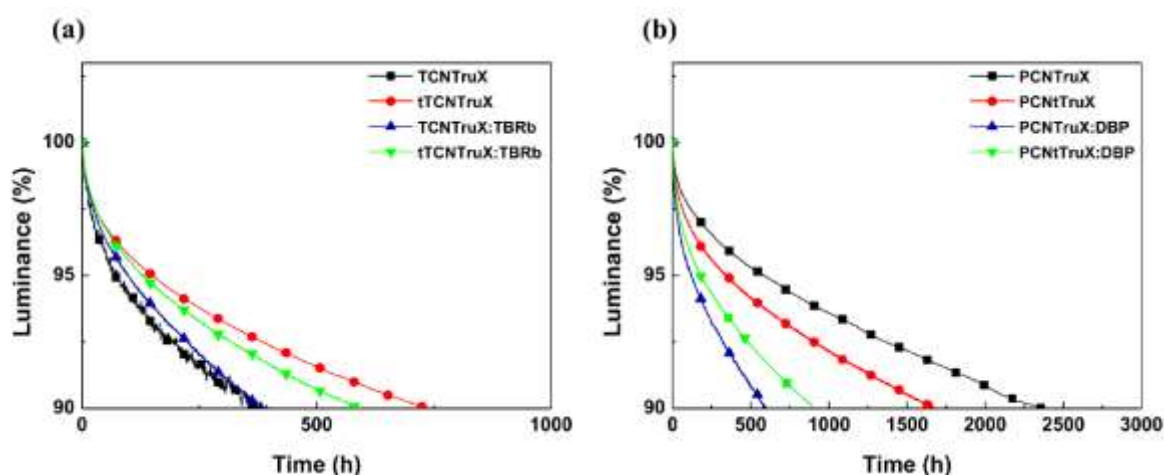


Figure 8. Device operational lifetime curves of (a) **TCNTruX**, **tTCNTruX** and (b) **PCNTruX**, **PCNtTruX** TADF and hyperfluorescence devices at an initial luminance 1000 cd m⁻².

Conclusions

In this work, three TADF materials were synthesized to study the effect of *tert*-butyl blocking groups on the EQE and device lifetime of the hyperfluorescence system. The *tert*-butyl unit managed the DET process from the TADF sensitizer to the fluorescent dopant, increasing the EQE and device operational lifetime in the yellow and red hyperfluorescence devices. Especially, **tTCNTruX** and **PCNtTruX** assisted hyperfluorescence devices demonstrated long device operational lifetime in the yellow and red hyperfluorescence devices, respectively. Therefore, the design of adding the *tert*-butyl blocking groups to the TADF sensitizer is effective to achieve high EQE and long device operational lifetime.

References

- [1] Uoyama H, Goushi K, Shizu K, Nomura H, Adachi C. Highly efficient organic light-emitting diodes from delayed fluorescence. *Nature*. 2012;492(7428):234-8.
- [2] Kaji H, Suzuki H, Fukushima T, Shizu K, Suzuki K, Kubo S, et al. Purely organic electroluminescent material realizing 100% conversion from electricity to light. *Nat. Commun*. 2015;6(1):8476.
- [3] Dias FB, Bourdakos KN, Jankus V, Moss KC, Kamtekar KT, Bhalla V, et al. Triplet Harvesting with 100% Efficiency by Way of Thermally Activated Delayed Fluorescence in Charge Transfer OLED Emitters. *Adv. Mater*. 2013;25(27):3707-14.
- [4] Adachi C. Third-generation organic electroluminescence materials. *Jpn. J. Appl. Phys*. 2014;53(6):060101.
- [5] Stewart DJ, Dalton MJ, Long SL, Kannan R, Yu Z, Cooper TM, et al. Steric hindrance inhibits excited-state relaxation and lowers the extent of intramolecular charge transfer in two-photon absorbing dyes. *Phys. Chem. Chem. Phys*. 2016;18(7):5587-96.
- [6] Bässler H, Schweitzer B. Site-Selective Fluorescence Spectroscopy of Conjugated

Polymers and Oligomers. *Acc. Chem. Res.* 1999;32(2):173-82.

[7] Nakanotani H, Higuchi T, Furukawa T, Masui K, Morimoto K, Numata M, et al. High-efficiency organic light-emitting diodes with fluorescent emitters. *Nat. Commun.* 2014;5(1):4016.

[8] Byeon SY, Lee DR, Yook KS, Lee JY. Recent Progress of Singlet-Exciton-Harvesting Fluorescent Organic Light-Emitting Diodes by Energy Transfer Processes. *Adv. Mater.* 2019;31(34):1803714.

[9] Zhang D, Song X, Cai M, Duan L. Blocking Energy-Loss Pathways for Ideal Fluorescent Organic Light-Emitting Diodes with Thermally Activated Delayed Fluorescent Sensitizers. *Adv. Mater.* 2018;30(6):1705250.

[10] Chan C-Y, Cui L-S, Kim JU, Nakanotani H, Adachi C. Rational Molecular Design for Deep-Blue Thermally Activated Delayed Fluorescence Emitters. *Adv. Funct. Mater.* 2018;28(11):1706023.

[11] Kim JH, Lee KH, Lee JY. Design of thermally activated delayed fluorescent sensitizers for high efficiency over 20% and long lifetime in yellow fluorescent organic light-emitting diodes. *J. Mater. Chem. C.* 2020;8(15):5265-72.

[12] Song W, Lee JY. Design of a novel triplet exciton guiding mixed host for lifetime improvement of phosphorescent organic light-emitting diodes. *Org. Electron.* 2017;51:1-5.

[13] Lee Y, Woo S-J, Kim J-J, Hong J-I. Blue thermally activated delayed fluorescence emitter using modulated triazines as electron acceptors. *Dyes Pigm.* 2020;172:107864.

[14] Masui K, Nakanotani H, Adachi C. Analysis of exciton annihilation in high-efficiency sky-blue organic light-emitting diodes with thermally activated delayed fluorescence. *Org. Electron.* 2013;14(11):2721-6.

[15] Furukawa T, Nakanotani H, Inoue M, Adachi C. Dual enhancement of

electroluminescence efficiency and operational stability by rapid upconversion of triplet excitons in OLEDs. *Sci. Rep.* 2015;5(1):8429.

Accepted Manuscript